Applied Materials Today 30 (2023) 101730

Contents lists available at ScienceDirect

Applied Materials Today

journal homepage: www.elsevier.com/locate/apmt

ImmunoInertial microfluidics: A novel strategy for isolation of small EV subpopulations

Sajad Razavi Bazaz [a,1], Sareh Zhand [a,1], Robert Salomon [b], Elham Hosseini Beheshti [c,d], Dayong Jin [b], Majid Ebrahimi Warkiani [a,b,e,*]

[a] School of Biomedical Engineering, University of Technology Sydney, Sydney, NSW 2007, Australia
[b] Faculty of Science, Institute for Biomedical Materials and Devices, University of Technology Sydney, NSW 2007, Australia
[c] School of Medical Sciences, Faculty of Medicine and Health, The University of Sydney, Camperdown, NSW, Australia
[d] The Sydney Nano Institute, The University of Sydney, Sydney, NSW 2006, Australia
[e] Institute of Molecular Medicine, Sechenov First Moscow State University, Moscow 119991, Russia

ARTICLE INFO

Keywords:
Extracellular vesicle
Exosome
sEV subpopulation
Microfluidics
ImmunoInertial microfluidics

ABSTRACT

Cancer-specific small extracellular vesicles (sEVs), known as exosomes, have shown a great promise to serve as novel biomarkers for cancer diagnosis and prognosis in liquid biopsies. However, the high heterogeneity of sEVs posed great technical challenges to acquiring their molecular information. A simple and reproducible method for isolating subpopulations of sEVs can significantly enhance the detection and stratification of these circulating biomarkers and their function. This study used the synergic effects of the immunoaffinity-based approach and inertial microfluidics (ImmunoInertial microfluidics) to isolate specific subpopulations of sEVs. At first, the cancer cell-derived sEVs were captured on microbeads of varying sizes which were functionalized with specific capture antibodies such as epithelial cell adhesion molecule (EpCAM), epidermal growth factor receptor (EGFR), and the programmed death-ligand 1 (PD-L1), facilitating the selective capture of sEVs. The sEVs-bearing microbeads were subsequently introduced to a series of inertial microfluidic channels, called iZExoSub (inertial zigzag microfluidics for exosome subpopulation separation), for size-based bead separation. Results revealed more than 90% efficiency in sEVs subpopulation separation, further proved via flow cytometry analysis data. Our approach is capable of selective isolation and quantitative detection of important biomarkers from sEVs subpopulations with high sensitivity and low cost and has the capacity to process samples of varying volumes, ranging from μL up to mL continuously. This system can outperform FACS machines in terms of sample throughput by orders of magnitudes. In addition, this study emphasized the necessity of using a consistent sEV marker (as capture and detector) across different samples for accurate assessment of subpopulations.

1. Introduction

Extracellular vesicles (EVs) are lipid-membrane enclosed particles whose main biological relevance is conferred by their molecular content. The small EVs (sEVs) are a subset of EVs (30–150 nm in diameter) mainly originated from the endolysosomal pathway [1] and released from almost all cell types into the extracellular milieu [2]. They are found in nearly all biological fluids, including blood, saliva, urine, semen, sputum, breast milk, and cerebrospinal fluid [3–7]. The sEVs contain bioactive molecules such as enzymes, proteins, lipids, a variety of RNAs (mRNA, microRNA, and other non-coding RNAs), DNA, and other molecules. The molecular cargo of EVs resembles their cell of origin and reflects the real-time state of the parent cells, providing broad non-invasive access to substantial information regarding cell types in the human body that are otherwise inaccessible to biopsy [8]. Since sEVs carry host and pathogen-derived genomic, proteomic, and lipidomic cargos from their cells of origin [9], they can selectively transfer biologically active substances to the target cells they fuse with and used as cell signal transduction and are recognized as a novel mechanism of cell-to-cell communication [10,11]. This makes sEVs isolation crucial for diagnostic purposes in various diseases [12,13], including cancer, infectious, cardiovascular, or neurodegenerative diseases [14–16].

* Corresponding author at: School of Biomedical Engineering, University of Technology Sydney, Sydney, NSW 2007, Australia.
E-mail address: majid.warkiani@uts.edu.au (M.E. Warkiani).
[1] These authors contributed equally to this work.

https://doi.org/10.1016/j.apmt.2022.101730
Received 16 August 2022; Received in revised form 22 December 2022; Accepted 30 December 2022
Available online 7 January 2023
2352-9407/© 2023 Elsevier Ltd. All rights reserved.

In the minimal information for studies of extracellular vesicles (MISEV) 2018 position statement published by the International Society of Extracellular Vesicles, the guideline strongly recommended using the operational terms based on size [e.g., small (s), medium (m), or large (l) EVs], biochemical composition (e.g., CD63+ EVs), density range (e.g., low-, medium-, or high-density EVs), or culture- or cell type of origin (e.g., hypoxic EVs, cancer cell-derived EVs, etc.), unless the biogenesis of the EVs was determined [17]. However, many of these terms are protocol-dependent and a clear definition is required. Here, we use the term "sEVs" to refer to samples enriched in small EVs.

Since the EVs generated by cancer cells can be found in the circulation, there have been efforts to isolate them and analyze their contents as a form of liquid biopsy. There is growing evidence that tumor-derived sEVs contribute to promoting all the hallmarks of cancer: cell death resistance, sustained proliferation, evasion from growth suppression, angiogenesis, invasiveness and metastasis, genomic instability, and inflammation. The role of tumor-derived sEVs in the development and progression of several types of cancer is well established [18,19]. In this context, studies have confirmed that the major immune response regulator, i.e., programmed death-ligand 1 (PD-L1), is significantly enriched in metastatic melanoma cell-derived sEVs, compared to sEVs derived from the less aggressive cells [20], and the levels of exosomal PD-L1 correlate with the progression of head and neck squamous cell carcinoma [21]. Furthermore, the epithelial cell adhesion molecule (EpCAM, also known as CD326) represents a suitable candidate for cancer biomarker as it is overexpressed in many human adenocarcinomas and squamous cell carcinomas (29). It has also been shown that the level of exosomal EpCAM is positively correlated with the ovarian cancer stage and aggressiveness [22]. EpCAM is thus an appealing candidate biomarker for cancer diagnosis and the evaluation of anti-tumor therapy responses. Emerging evidence indicates the overexpression of the epidermal growth factor receptor (EGFR) drives tumor progression in several cancers, including breast, lung, glioblastoma, and head and neck cancers [23]. Therefore, the investigation through these markers can provide an insight into a cancer diagnosis/prognosis approach.

Several challenges hampered the utility of sEVs as biomarkers. SEVs are heterogeneous [24,25], making their isolation and analysis difficult. The heterogeneity of sEV populations has hindered our understanding of their molecular composition, biodistribution, and functions. Techniques such as centrifugation, precipitation, immunoaffinity capture, ultrafiltration, asymmetric-flow field-flow fractionation, and size exclusion chromatography have been developed for sEV isolation based on either size differences between EVs or targeting specific surface markers [26–28]. These methods enrich many kinds of sEVs found in the sample, representing highly heterogeneous populations of sEVs secreted from cell types. However, a large mixture of sEV types from different cellular origins can interfere with immunoassays. For this reason, a simple and reproducible method for isolating a specific subpopulation of sEVs can significantly enhance the detection of sEV-associated protein biomarkers.

Recently, microfluidic techniques have been proven to improve sEV isolation [29,30]. These devices reduce sample consumption, accelerate the reaction speed, can be multiplexed, and have high separation efficiency [31,32]. Microfluidic immunoaffinity-based methods have been developed recently, capable of isolating a specific subpopulation of sEVs by relying on the expression of the EV-specified surface markers. However, the throughput in these methods is extremely low (in the order of μL/hr) [33]. Inertial microfluidics represents a powerful tool for the size-based separation of particles with high throughput that can be incorporated for cell and EV separation [34,35]. However, the combination of microfluidic immunoaffinity-based approaches with inertial microfluidic systems (ImmunoInertial microfluidics) for the isolation of sEV subpopulations has never been reported, and this field of study is intact. This combined technique benefits from rapid and efficient sample processing along with the high selectivity of the obtained sEV subpopulations.

Here for the first time, we have utilized ImmunoInertial microfluidics to isolate marker-specific sEVs. The proposed technique is capable of isolating sEV subpopulations enriched in specific markers from cell culture condition media or biological fluids. In this method, beads of different sizes were first functionalized with an individual set of capturing antibodies against tetraspanins (CD81, CD9, and CD63) as well as EpCAM, PD-L1, and EGFR to facilitate the selective capture of sEVs. The sEV-bearing beads were then separated based on their sizes using inertial microfluidics in a series of rigid zigzag microchannels called iZExoSub (Inertial Zigzag microfluidics for Exosome Subpopulation separation). The separated sEVs were further characterized using flow cytometry. In this study, we have set up a new methodological approach by which one or more specific subpopulations of sEVs can be conveniently and comprehensively investigated, consequently offering novel phenotypic and functional insights applicable for cancer early diagnosis, prognosis, and monitoring the patient's response to chemotherapy/immunotherapy.

2. Materials and methods

Part of the experimental information is described in the supplementary information.

2.1. Device fabrication

The microfluidic devices used in this study were fabricated using our previously established 3D printing method [36]. In brief, channels are first drafted by a commercial CAD drawing software (SolidWorks 2021) and exported as an STL file to become a readable format for the 3D printer. The file is then sliced in the Z direction using the Miicraft software (Version 6.3.0.t3, Miicraft). The structure is fabricated layer by layer on a build plate when the UV light with a wavelength of 358–405 nm is projected from the bottom of the resin bath (filled with BV-007 resin) and passes through a transparent Teflon film. Once the UV light cures one layer, the Z-stepper motor moves one slice upward, and the next layer starts to be polymerized [37]. This process continues until the part is printed successfully. After the part is printed and removed from the picker, it should be washed with isopropanol (IPA) and air-dried by an air-gun, followed by 30 s post-curing by exposing to a UV light with 405 ± 5 nm wavelength. Finally, tubes were connected to the microchannel.

2.2. Evaluation of the iZExoSub for particle separation

In order to find out the efficiency of the iZExoSub for separating distinct-size beads, the high-speed camera, fluorescent imaging of fluorescent-labelled particles, and counting the number of cells in each outlet were used. The mixed population of beads was assessed before and after passing through the microfluidic device over a variety of flow rates, and the separation efficiency was evaluated. Depending on the number of sEVs and the number of channels used, the microchannel has been evaluated over wide ranges of flow rates.

2.3. Cell culture conditioned media preparation and extracellular vesicle isolation

Human breast cancer cell line (MCF-7), human lung cancer cell line (A549), and MCF-7 cells that previously co-cultured with human epithelial fibroblast (MCF-7/fibroblast) cells to make the MCF-7 cells express the PD-L1, were used for this study. The detailed culture conditions are described in supplementary information Section S2. For the conditioned media preparation, the cells were cultured in an EV-free medium under hypoxic conditions for 48 h at 37°C in a 5% CO_2 humidified incubator. Media containing released EVs was collected and subjected to multiple centrifugation and ultracentrifuge steps to isolate sEVs. The detailed steps are described in supplementary information

Section S4. The isolated sEVs were quantified using nanoparticle tracking analysis, western blotting, scanning electron microscopy, and transmission electron microscopy (Supplementary information Sections S5-S8).

2.4. Optimized antibody immobilization strategy

For antibody immobilizations on the surface of carboxylate polystyrene beads, four different techniques, including Mix&Go kit, Dynabeads antibody coupling kit, EDC, and EDC/sulfo NHS, were tested to find the best approach in terms of binding strength in total sEVs count. The detailed steps are described in the supplementary information section S9. The functionalized beads with four different techniques were decorated with ani-CD63 antibody and separately incubated with the 2.5 μg of MCF-7 and/or A549 cell-derived sEVs for 18 h at 4°C without agitation. In the control group, bovine serum albumin (BSA) was used instead of sEVs. Excess non-reacted sEVs were removed by centrifugation at 3000×*g* for 5 min. The labeled anti-CD63 APC (353,008, Biolegend, USA) detection antibody was then added to the tubes and co-incubated for 90 min at 37°C. Following three times washing steps, the mixture was re-suspended in 1 mL of PBS and subjected to flow cytometry analysis (CytoFLEX LX, Beckman Coulter, USA). Gates were set on the bead fraction visible in the FSC/SSC light scatter. The histogram was drawn for all the polystyrene beads functionalized with antibodies using CytExpert V 2.4 or FlowJo V 10 software. The results were repeated after a week to examine the stability of the antibody attachment on the surface of beads. Also, results were repeated using different batches of beads to evaluate the reproducibility of the method.

2.5. Assessing the efficiency of iZExoSub on separating two distinct size beads containing target sEVs

In the next step, the separation efficiency of the iZExoSub for two distinct-size beads containing target sEVs was evaluated (the schematic process is provided in Fig. 4A and B). In this study, the sEVs expressing EpCAM were separated from sEVs that do not express this biomarker. To this end, 1 mg of 3 and 10 μm carboxylate polystyrene beads were functionalized with EDC/sulfo NHS separately and decorated with human anti-CD63 antibody. Then, the 3 and 10 μm functionalized beads with anti-CD63 were incubated with 2.5 μg of A549-derived sEVs (as EpCAM negative, Supplementary information section S13) and the MCF-7 cell-derived sEVs (as EpCAM positive, Supplementary information Section S13), respectively. In the control group, BSA was used instead of sEVs. The complex contained sEV- bearing beads were then introduced into the iZExoSub microdevice (single channel) at the flow rate of 1 mL/min. Each outlet was divided into two separate microtubes, one co-incubated with the labeled detection anti-EpCAM-PE/Dazzle™ 594, and the other one with anti-CD63-APC antibody for 90 min at 37°C. Next, the complexes were washed 3 times with PBS, re-suspended in 1 mL of PBS, and subjected to flow cytometry (CytoFLEX LX, Beckman Coulter, USA). The concentration of antibody and the number of beads was kept constant in all steps [3 μg antibody per 1 mg of 3 μm beads (1.87×10^{14}), and 4 μg antibody per 1 mg (1.87×10^{6}) of 10 μm beads]. A control for flow cytometry machine was prepared, including the 3 and 10 μm beads incubated with BSA and anti-EpCAM-PE/Dazzle™ 594, as well as the mixture of 3 and 10 μm beads with BSA and anti-CD63-APC antibody. The 10,000 events were acquired. Gates were set on the bead fraction visible in the FSC/SSC light scatter. The histogram was drawn for all the polystyrene beads functionalized with antibody using CytExpert V 2.4 or FlowJo V10 software.

2.6. Assessing the efficiency of iZExoSub on separation of three beads containing the target sEVs

In this study, the sEVs expressing three cancer protein markers, including EpCAM, PD-L1, and EGFR were studied which derived from MCF-7, A549, and MCF-7/fibroblast cell lines, respectively.

To find out the separation efficiency of the iZExoSub, 1 mg of 3, 10, and 20 μm carboxylate polystyrene beads were functionalized with EDC/sulfo NHS separately and decorated with anti- human PD-L1, anti-human EpCAM, and anti-human EGFR antibody, respectively (the detailed method of antibody immobilization is described in Supplementary information section S9). Then, the functionalized beads were incubated with 2.5 μg of the mixture of MCF-7/fibroblast cell-derived sEVs (as PD-L1 positive, Supplementary information Section S13), MCF-7 cell-derived sEVs (as EpCAM positive, Supplementary information Section S13), and A549 derived EVs (as EGFR positive, Supplementary information Section S13), for 18 h at 4°C without agitation. In the control group, BSA was used instead of sEVs. Excess non-reacted sEVs were removed by centrifugation at 3000×*g* for 5 min. The mixtures containing sEV-bound microbeads were then introduced to the iZExoSub for size-based bead separation (Fig. 1). In the iZExoSub microfluidic device, the EV-bearing beads were separated in two steps. Each outlet was then divided into four separate microtubes co-incubated with the labeled detection anti-EpCAM-PE/Dazzle™ 594, anti-CD63-APC, anti-human EGFR-Alexa Fluora 488, and anti-PD-L1-PE/Cy7 antibody for 90 min at 37°C. Next, the complexes were washed 3 times with PBS and re-suspended in 1 mL of PBS and subjected to flow cytometry (CytoFLEX LX, Beckman Coulter, USA). The concentration of antibody and the number of beads was kept constant in all steps (3 μg antibody per 1 mg (1.87×10^{14}) of 3 μm beads, 4 μg antibody per 1 mg (1.87×10^{6}) of 10 μm beads, and 6 μg antibody per 1 mg (1.87×10^{3}) of 20 μm beads). Four control groups for the flow cytometry machine were prepared, including the mixture of 3, 10, and 20 μm beads with BSA, the mixture of 3, 10, and 20 μm beads with BSA and anti-human EGFR- Alexa Fluora 488, the mixture of 3, 10, and 20 μm beads with BSA and anti-EpCAM-PE/Dazzle™ 594, the mixture of 3, 10, and 20 μm beads with BSA and anti-PD-L1-PE/Cy7, and the mixture of 3, 10, and 20 μm beads with BSA and anti-CD63-APC antibody (the schematic process is provided in Fig. 5A).

3. Results and discussion

3.1. ImmunoInertial microfluidics principles

Improvements in developing new strategies to isolate specific subpopulations of sEVs quickly and sensitively will facilitate the practical application of EV-based liquid biopsy for cancer precision medicine. The ImmunoInertial microfluidics technique can assist in achieving this aim. This methodology contains two functional compartments: 1) sEVs immobilization onto microbeads and 2) size-based separation of sEV captured microbeads. (Fig. 1). The technique we employ for microbead separation is based on inertial microfluidics, which proves to be an ideal candidate for the size-based separation of cells and particles [34,38]. The method is high-throughput (more than 1000 times faster than other available techniques like deterministic lateral displacement or viscoelastic fluids) [39], robust, clog-free, and has a high degree of separation and purification efficiency. The purified specific sEV subpopulations can further be applied for various diagnostics, prognostics, or therapeutics purposes.

3.2. Characterization of sEVs

The particle size and concentration of sEVs derived from A549, MCF7, and MCF7/fibroblast cell lines were characterized using NTA complemented with Western Blot, SEM, and TEM (Fig. 2 A–D). The size distribution of sEVs derived from A549, MCF7, and MCF7/fibroblast measured by NTA showed a peak at 128.1 +/- 8.2 nm (A549), 147.8 +/- 6.9 nm (MCF7), and 112.0 +/- 3.7 nm (MCF7/fibroblast); most of the particles had a mean size of 100–200 nm (Fig. 2A). The concentration of 5×10^{10} particles/ml, 1.3×10^{11} particles/ml, and 2.1×10^{11} particles/ml was determined for sEVs enriched from MCF-7/fibroblast, A549, and MCF-7 cells, respectively. The immunofluorescence staining and flow

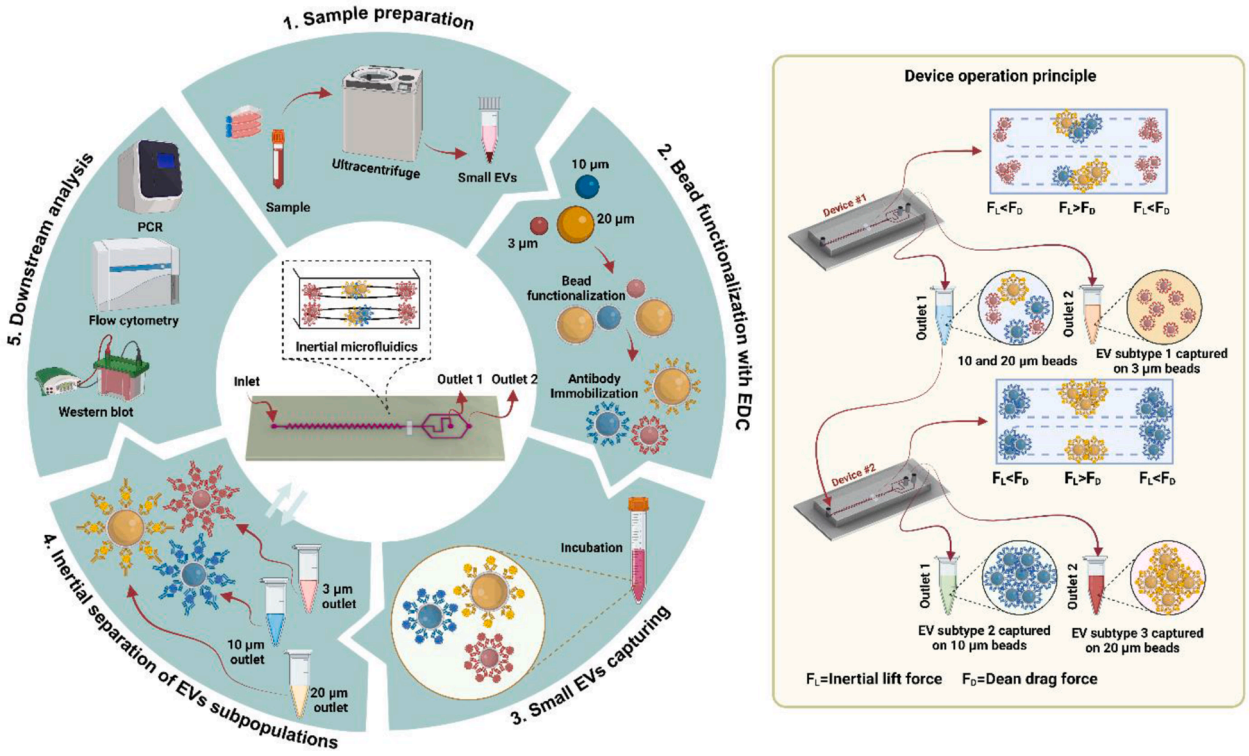

Fig. 1. ImmunoInertial microfluidics workflow. Schematic illustration of ImmunoInertial microfluidics workflow, comprising five steps from the sample collection to downstream analysis. The method is capable of isolating sEV subpopulations from different sources at large-scale.

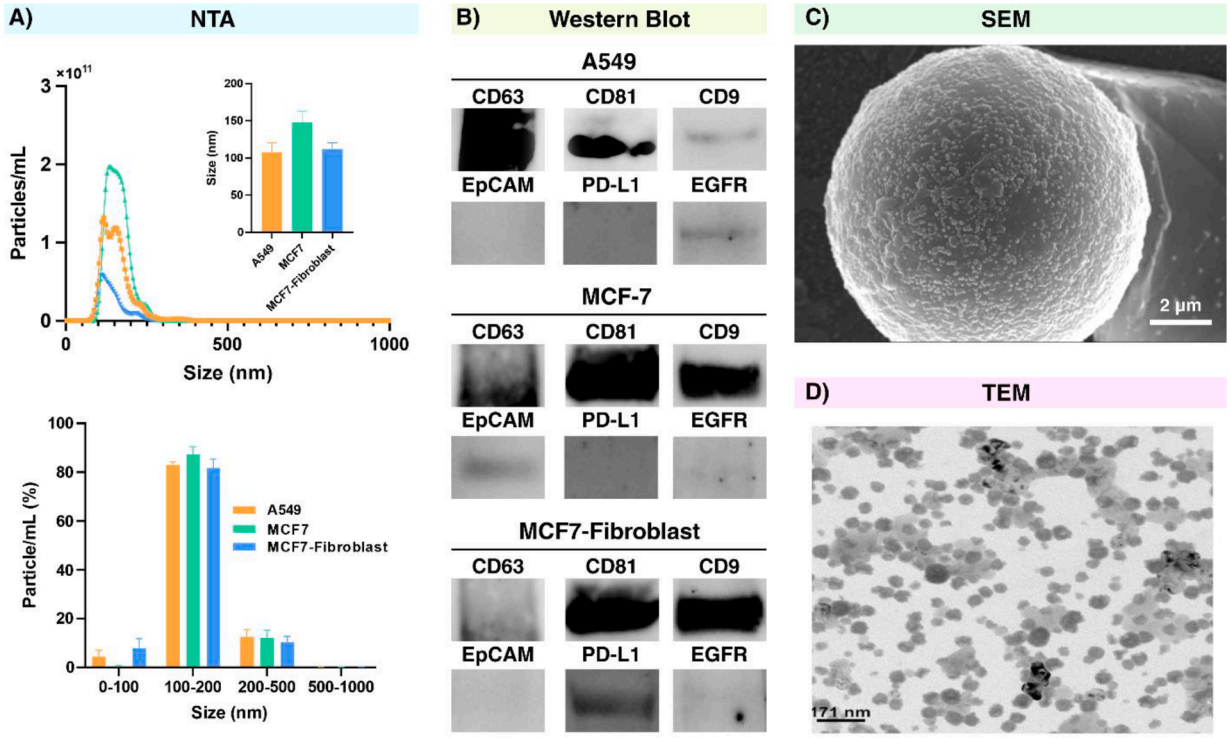

Fig. 2. sEV characteristics. (A) Nanoparticle tracking analysis of sEVs derived from A549, MCF-7, and MCF-7/fibroblast cell culture supernatant. (B) In Western Blot analysis, sEVs were loaded on SDS-PAGE and immunoblotted for antibodies against tetraspanins (CD9, CD63, and CD81) as well as anti-PD-L1, anti-EpCAM, and anti-EGFR. A gel was run under non-reducing and reducing conditions with 2×10^8 particles; ~5 µg sEVs. The exposure time was 35 s. (C) SEM images of 10 µm polystyrene bead covered with sEVs at 2000x magnification (Scale bar: 2 µm). The bead was functionalized with anti-CD63 capture antibody. (D) TEM images of sEVs isolated from MCF-7 cell culture supernatant.

cytometry analysis of the A549, MCF-7, and MCF-7/fibroblast cells show high expression of EGFR in A549 cells, EpCAM in MCF-7 cells, and PD-L1 in MCF-7/fibroblast cells (Fig. S1). Thus, it is concluded that the sEVs derived from the above-mentioned cells can express these markers as well. The tetraspanins (CD63, CD81, and CD9) were detected in the sEVs derived from studied cell lines using Western Blotting. The EGFR protein was expressed in sEVs derived from A549 cells but not in two other cells, which is consistent with our flow cytometry analysis (Fig. S2C). In agreement with our flow cytometry analysis, our Western Blotting demonstrates EpCAM expression on sEVs derived from MCF-7 cells and PD-L1 expression on sEVs derived from MCF-7/fibroblast cells (Fig. 2B). The SEM image of 10 μm polystyrene bead functionalized with anti-CD63 antibody and covered with sEVs confirms the maximum binding efficiency of the antibodies on the carboxylate polystyrene beads using EDC/sulfo NHS (Fig. 2C). Furthermore, the TEM image of sEVs showed their expected size and morphology (Fig. 2D).

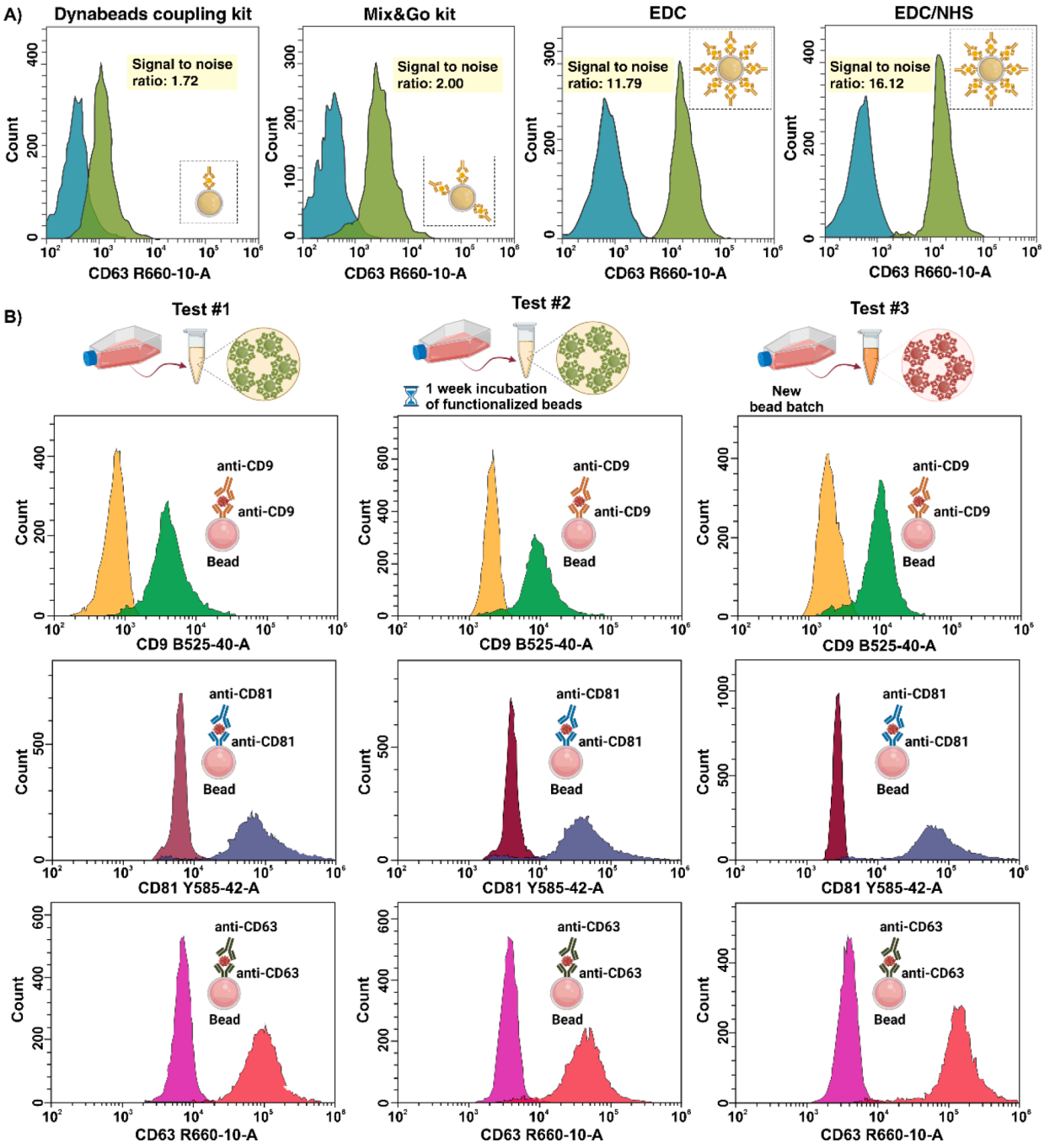

Fig. 3. Immunoaffinity characterization. (A) comparison of various strategies for antibody immobilization on the carboxylate polystyrene beads. Dynabeads antibody coupling kit and Mix&Go kit do not show proper sEVs binding efficiency (low signal to noise ratio), both EDC and EDC/sulfo NHS confirmed >98% sEVs binding efficiency (high signal to noise ratio). In all experiments, the MCF-7 cell-derived sEVs were used and in the control group, BSA was used instead of sEVs (blue histogram). (B) Test #1 Flow cytometry analysis for evaluating the efficiency of EDC/sulfo NHS chemistry for anti-CD9, -CD81, and -CD63 antibody attachment on beads. (Test 2#) Stability of anti-CD9, -CD81, and -CD63 antibodies attachment on beads over a time, and (Test #3) reproducibility of anti-CD9, -CD81 and -CD63 antibodies attachment on beads using new batches of beads. The results confirm that the antibody attachment on the beads is stable over time with limited batch-to-batch variability. In all experiments, the MCF-7 cell-derived sEVs were used and in the control group, BSA was used instead of sEVs (yellow histogram in CD9, red histogram in CD81, and purple histogram in CD63).

3.3. Efficient antibody immobilization technique

To maximize the immune-capture efficiency, the stability of the antibody on the functionalized beads as well as the reproducibility of the immobilization were evaluated. The signal-to-noise ratio was calculated by subtracting the mean fluorescence intensity (MFI) of the positive fluorescent signal from the APC channel (for the detection of anti-CD63 APC) from MFI of the background and dividing to the two times standard deviation of the APC channel. Results indicate that the Dynabeads antibody coupling and Mix&Go kit are inappropriate for our application due to the low signal-to-noise ratio (Fig. 3A), although they are widely used in the literature [40–42]. Results indicate that by applying the EDC and EDC/sulfo-NHS chemistry to the carboxylate polystyrene beads, the signal-to-noise ratio for the anti-CD63 immobilization efficiency increases to 11.79 and 16.12, respectively (Fig. 3A), signifying the maximum binding efficiency of sEVs per microbead for the two above-mentioned strategies.

Our flow cytometry analysis using anti-CD63 as a capture antibody and anti-CD63-APC detector antibody revealed that sEVs derived from the MCF-7 cell line expressed CD63 marker (Fig. 3B). Moreover, three common EV markers (CD9, CD81, and CD63) are stable on the surface of functionalized beads after a week (Fig. 3B). Results of flow cytometry analysis using different batches of beads functionalized with antibodies shows neglectable batch-to-batch variability of the antibody immobilization strategy (Fig. 3B). Similar results were achieved using A549 and MCF-7/fibroblast cell-derived sEVs (Fig. S2 A, B) as well as applying tetraspanins as a capture antibody and anti-EpCAM-PE/Dazzle™ 594 for the detection in MCF-7 cell-derived sEVs (Figs. S2 A, B and S3). The results confirmed the stability and reproducibility of the EDC/sulfo NHS for immunoaffinity purification of sEV subpopulations.

3.4. Performance of iZExoSub for particle separation

To separate beads of different sizes, we have used the iZExoSub microfluidic device. This device relies on inertial and Dean drag forces to separate particles based on their sizes. The fundamentals and principles of particle and cell focusing within rigid zigzag microchannels have been recently evaluated by our group [43]. In these channels, Reynolds number is in the intermediate range ($1<Re<100$), between the Stokes and turbulent flow regimes, the fluid regime is laminar. In this regime, inertial forces (F_L) assist in focusing randomly dispersed particles toward certain equilibrium positions. Within a straight channel, shear-gradient and wall-induced lift forces are the main forces that affect particles. In iZExoSub, Dean force (F_D) is introduced differently compared to the spiral microfluidic channel. The interchanging channel direction creates a mismatch of fluid flow velocity in an alternating pattern and introduces Dean force, accelerating the focusing of particles inside the channel.

A zigzag channel has three focusing modes across different flow rates. When $F_L < F_D$, the particles focus on the side of the channels. When $F_L > F_D$, the particles were focused on the middle of the channel due to the strong F_L. When $F_L \sim F_D$, particles are in the transition mode [43]. Particles can be separated based on their size if one is affected by F_L and the other is influenced by F_D. Based on the number of distinct size beads (n), we require microchannels (n-1) for the bead separation. For instance, for the separation of five distinct-size beads-bearing sEVs, four channels would be required. likewise, for the separation of three distinct size beads-bearing sEVs, two channels or two steps would be required. For this aim, we designed the channel in a way to focus the smallest bead on the channel side while all others focus in the channel center. The next channel will do the same until the separation of all particles (Fig. 1). One primary advantage of the zigzag channel is its operating range of flow rates, i.e., it can operate over a wide range of flow rates. Moreover, the channels are made from rigid materials, making them robust and not prone to swelling or inflation [36].

3.5. Performance of iZExoSub for the separation of two distinct size beads containing target sEVs

The workflow of the ImmunoInertial microfluidics technique for two distinct size beads containing target sEVs is illustrated in Fig. 4A. The particle trajectory of 3 and 10 μm beads is illustrated in Fig. 4B, where at the optimum flow rate (1 mL/min, Fig. 4C and D) 3 μm particles are under the influence of drag forces and occupied side walls. In contrast, 10 μm particles are governed by inertial lift forces and occupy the channel centerline. The flow cytometry dot plot showed the population percentage of 3 μm and 10 μm beads in each outlet, respectively (Fig. 4EI and 4EII). In both 3 μm and 10 μm outlets, the sEV-bearing beads express CD63, indicating the device does not have any negative effect on the sEVs, and the beads collected in both outlets had captured sEVs (Fig. 4EI and 4EII, insets). Also, the flow cytometry results revealed that in the 3 μm outlet, beads contain EpCAM negative sEVs as none of the beads show fluorescent intensity, and in the 10 μm outlet beads contain EpCAM positive sEVs as 54.1% of the beads-bearing sEVs express EpCAM (Fig. 4EIII and 4EIV).

3.6. Performance of iZExoSub for the separation of three distinct size beads containing target sEVs

Detection of biomarkers that are expressed in cancer cell-derived sEVs has significant potential for both diagnosis and treatment of cancer. These biomarkers are usually abundant in numbers and monitoring specific types of them can provide investigators with resourceful insights. Thus, developing an innovative assay enabling sEV separation based on protein profiling could offer in-depth analysis of molecular characteristics of sEVs and advance sEV-based liquid biopsies with improved accuracy for cancer detection and post-treatment prognosis.

The workflow of the ImmunoInertial microfluidics technique for the separation of three distinct-size beads containing target sEVs is illustrated in Fig. 5A. The beads were separated in two steps. In the first step, the 3 μm beads were separated from the 10 and 20 μm beads. In the next step, the 10 μm beads were separated from the 20 μm beads (Fig. 5A). Separation efficiency is determined by the percentage of microbeads retrieved from the target outlet to the total number of microbeads in the outlets. High separation efficiency means minimum loss of sEVs. The microbeads for each size were counted after collection from each outlet, and the separation efficiency was calculated as defined. The maximum separation efficiency for the 3 μm beads was obtained at the flow rate of 1 mL/min (Fig. 5B). As the driving force was sufficient at this flow rate of 1 mL/min, the 3 μm beads were focused at the side walls. In comparison, the 10 and 20 μm beads were focused at the middle of the channel because of considerably large inertial forces. Similarly, in the next chip, the maximum separation efficiency for the 10 μm and 20 μm beads was obtained at the flow rate of 0.8 mL/min (Fig. 5C).

Moreover, the flow cytometry results revealed that 73.71% of 3 μm beads captured by PD-L1 positive sEVs are expressing CD63, 92.78% of 10 μm beads captured by EpCAM positive sEVs are expressing CD63, and 78.32% of 20 μm beads captured by EGFR positive sEVs are expressing CD63 (Fig. 5D). The isolated sEVs can further be used for post analysis using flow cytometry, genomics, and proteomics analysis of EV content.

Various microfluidic devices for sEV enrichment or subpopulation separation have been invented during the past decade. Among them, the microfluidic-based immunoaffinity technique is of great interest. Therefore, various microfluidic devices including EVs on demand chip (EVOD) [44], ExoChip [45], size-based exosome total isolation chip (ExoTIC) [46], ExoSearch [47], Deterministic lateral displacement (DLD chip) [48], exosome-specific dual-patterned immunofiltration (ExoDIF) [49], exosome detection method via the ultrafast-isolation system (EXODUS) [50], and nano-wire-based exosome separation device [51] have been developed. However, most of these methods are low throughput, recovery, and purity and suffer from prolonged sample processing time. Also, they are prone to clogging, and sEV isolation

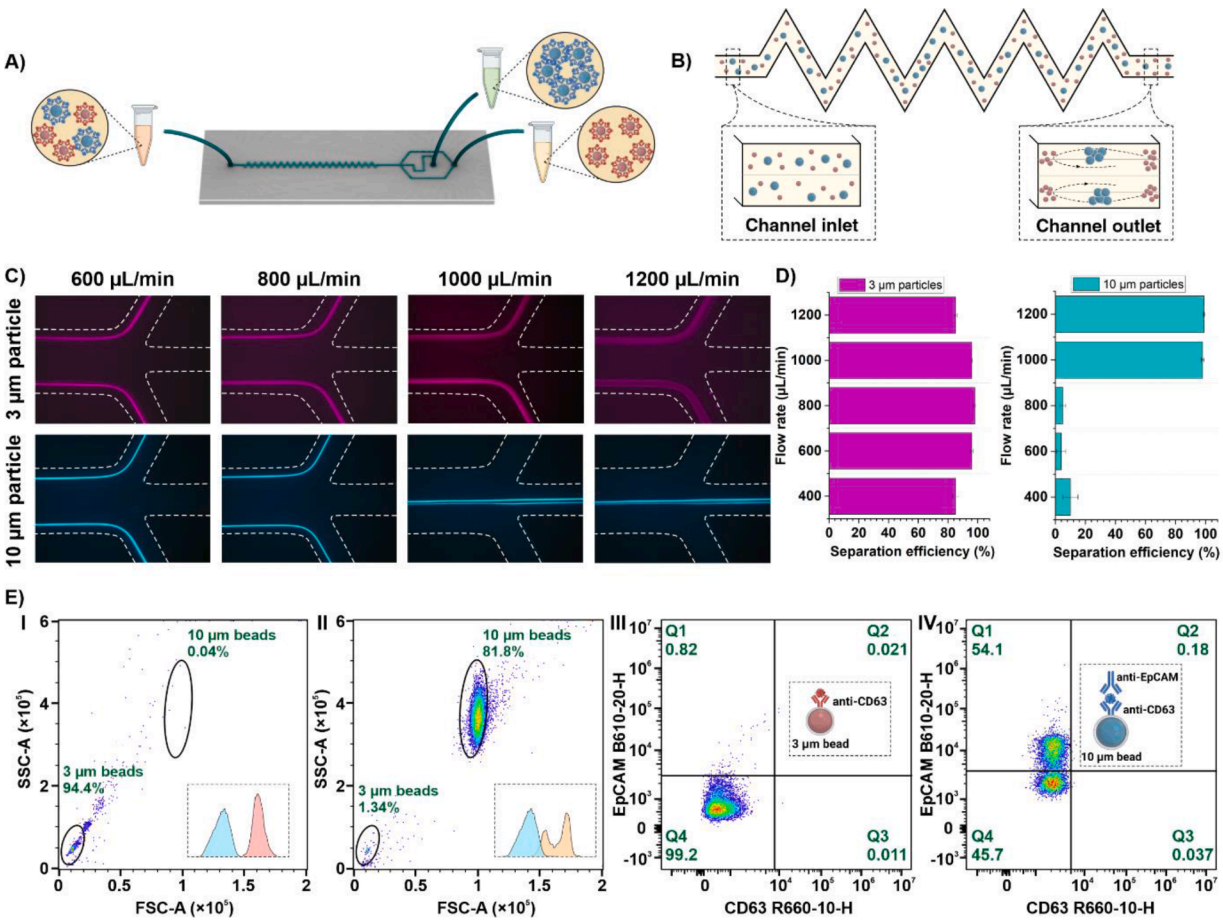

Fig. 4. Separation of two distinct size beads containing target sEVs. (A) The schematic illustration of the ImmunoInertial microfluidics technique for the separation of two distinct-size beads containing target sEVs. (B) The trajectory of different particles passing through the channel. Small particles are focused on the channel side due to the dominant effects of inertial lift forces, while large particles are focused on the channel center. (C) Fluorescent streaks for 3 and 10 µm particles at the channel outlet. Results show that for the channel with a hydraulic diameter of ~ 69 µm and aspect ratio of ~ 0.16, 3 µm particles are focused on the channel sidewalls over wide ranges of flow rates, 600–1200 µL/min, while 10 µm particles are first focused on the channel sidewalls and then focused at the channel center. 1000 µL/min for two distinct-size beads containing target sEVs. (D) Separation efficiency of 3 and 10 µm particles versus different flow rates. At 1000 µL/min, separation efficiency for both 3 and 10 µm particles is more than 95%. (E) I and II demonstrate flow cytometry data for separating 3 and 10 µm sEV-bearing beads after passing through the iZExoSub. The inset proves that we have captured sEVs from the samples. In the control group, BSA was used instead of sEVs (blue histogram). III and IV. The 3 µm beads contain sEVs that do not express EpCAM compared to the 10 µm beads that contain sEVs expressing EpCAM.

within the channel is troublesome and sometimes impossible to achieve. More importantly, most of them could separate only one subpopulation of sEVs based on protein marker. All these issues have been addressed in the ImmunoInertial microfluidics technique provided here (the actual device is shown in Fig. S4). Moreover, the developed technique is rapid; It can successfully separate three distinct size EV-bearing beads in less than 5 min for a 1 ml of any types of bodily fluids derived sEVs. The use of our iZExoSub can be expanded to separate up to five markers depending on the demands of clinical applications by designing the structure of the separation channel in series. These devices are inherently operated at high flow rates, they are usually clog-free with less chance of blockage or swelling. The iZExoSub channel proposed here is robust, made from rigid materials, and the operation is stable. The chemistry used for the immunoaffinity step is stable and does not demonstrate any degradation over the time or batch-to-batch variability.

Although there are multiple commercially available kits and sorting equipment enabling the isolation of specific subpopulation of sEVs based on the protein of interest, the existing kits fail the simultaneous multiplex separation of surface epitopes present on sEVs. Also, magnetic-activated cell sorting or fluorescent-activated cell sorting require adroit and experienced users and advanced facilities, and the efficiency always differs from person to person.

Cascading the microchannel for subsequent separation of sEVs, integrating the device with pumps, and using a micromixer for rapid binding of sEVs on functionalized beads are further improvements that can be applied to ImmunoInertial microfluidic technique which are currently under development by our group. It is worth mentioning that each inertial microfluidic system has a known capacity for bead handling; thus, a large bead population will result in focusing disturbance within the channel. In addition, the proposed workflow can be simplified by integrating certain signal detectors for on-chip cytometry detectors.

4. Conclusion

In this study, we have developed a highly efficient method to isolate specific subpopulation of sEVs using the synergistic effects of immunoaffinity and inertial microfluidics (ImmunoInertial microfluidics). The developed technique can successfully separate two, three, or more distinct size sEV-bearing beads rapidly with high degree of separation efficiency. The isolated sEVs can further be used for post-analysis using flow cytometry, genomics, and proteomics analysis of the sEV content. We are of the opinion that the ImmunoInertial technique can be used as a potent clinical tool for deep cancer characterization, providing insights into cancer management and monitoring its response to the treatments.

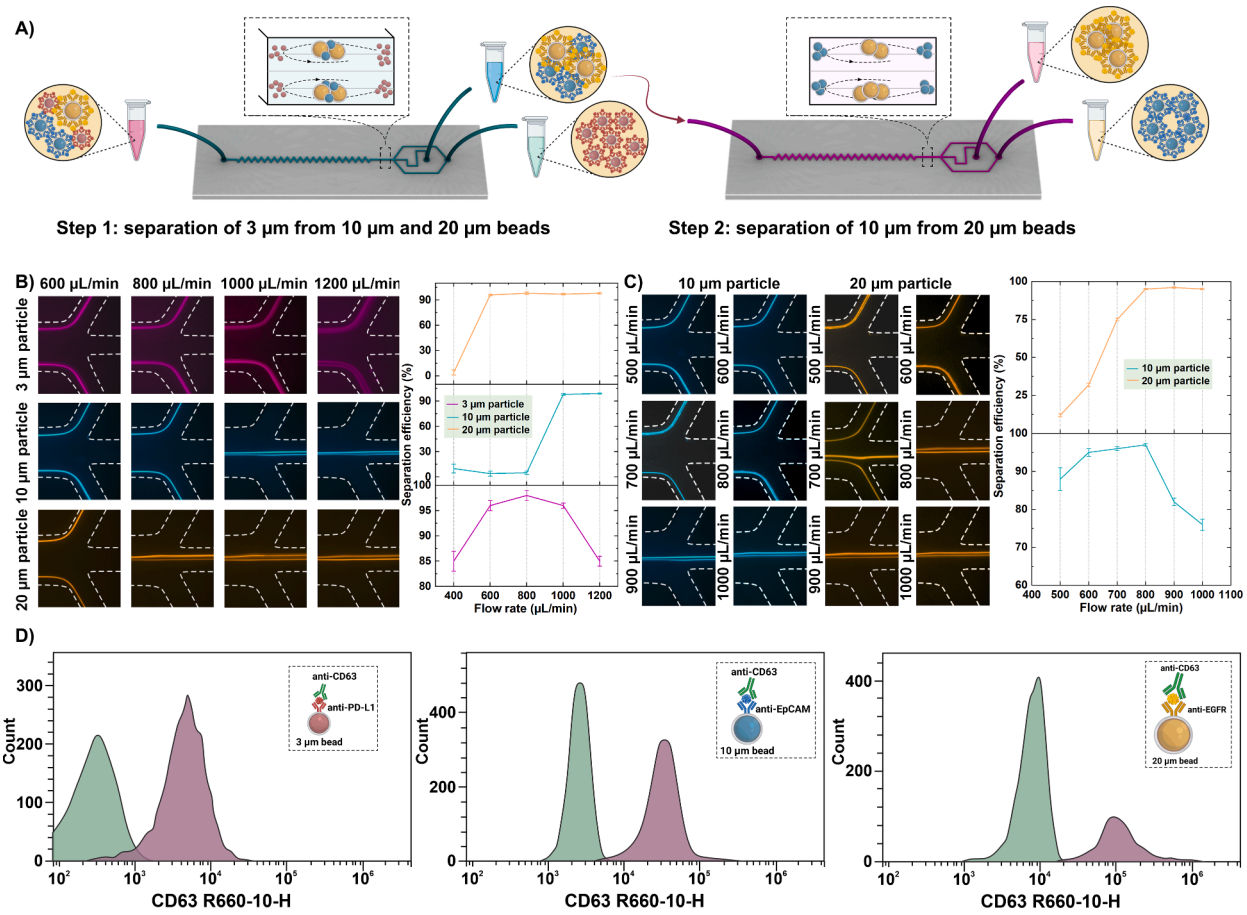

Fig. 5. Separation of three distinct size beads containing target sEVs. (A) The schematic illustration of the ImmunoInertial microfluidics technique for separating three distinct-size beads containing target sEVs. In the first step, 3 μm particles were separated from 10 to 20 μm ones, and in the second step, 10 μm particles were separated from 20 μm ones. (B) Fluorescent streaks of 3, 10, and 20 μm particles. The results show that the channel with a hydraulic diameter of ~ 69 μm and an aspect ratio of ~ 0.16 can focus 3 μm particles at the side walls while pushing 10 and 20 μm particles at the channel center. (C) Fluorescent streaks of 10 and 20 μm particles. The results show that the channel with hydraulic diameter of ~ 97.5 μm and aspect ratio of ~ 0.23 can separate 10 from 20 μm particles at flow rate of 800 μL/min (D) The expression of CD63 on the sEV-bearing beads captured with anti-EpCAM, anti-PD-L1, and anti-EGFR proves that we have successfully purified sEVs from the samples. In the control group, BSA was used instead of sEVs (green histogram).

Majid Ebrahimi Warkiani reports financial support was provided by University of Technology Sydney. Majid Ebrahimi Warkiani reports a relationship with Takeda Pharmaceutical that includes: funding grants. Majid Ebrahimi Warkiani reports a relationship with Cancer Institute NSW that includes: funding grants. Elham Hosseini Beheshti reports a relationship with New South Wales Dust Diseases Authority that includes: funding grants. Majid Ebrahimi Warkiani reports a relationship with Australia-China Joint Research center that includes: funding grants.

CRediT authorship contribution statement

Sajad Razavi Bazaz: Methodology, Software, Validation, Data curation, Investigation, Formal analysis, Writing – original draft, Writing – review & editing, Visualization. **Sareh Zhand:** Methodology, Validation, Investigation, Data curation, Formal analysis, Writing – original draft, Writing – review & editing. **Robert Salomon:** Data curation, Formal analysis, Writing – review & editing. **Elham Hosseini Beheshti:** Writing – review & editing. **Dayong Jin:** Supervision, Project administration, Funding acquisition. **Majid Ebrahimi Warkiani:** Conceptualization, Methodology, Supervision, Resources, Project administration, Funding acquisition.

Declaration of Competing Interest

The authors declare the following financial interests/personal relationships which may be considered as potential competing interests.

Data availability

Data will be made available on request.

Acknowledgement

M.E.W. would like to acknowledge the support of Takeda Pharmaceutical through the COCKPI-T Funding program and the Cancer Institute New South Wales through the Career Development Fellowship. EHB acknowledges the Dust Diseases Board competitive grant. The views expressed herein are those of the authors and are not necessarily those of iCare or the Dust Diseases Board. This work was performed in part at the South Australian node of the Australian National Fabrication Facility under the National Collaborative Research Infrastructure Strategy. The authors acknowledge the financial support from Australia-China Joint Research center for Point-of-Care Testing (ACSRF65827, SQ2017YFGH001190), Science and Technology Innovation Commission of Shenzhen (KQTD20170810110913065). The authors would like to acknowledge Hossein Ahmadi Nejad Joushani for his expertise and

assistance through the development of the microfluidic device.

Supplementary materials

Supplementary material associated with this article can be found, in the online version, at doi:10.1016/j.apmt.2022.101730.

References

[1] J. Morvan, B. Rinaldi, S. Friant, Pkh1/2-dependent phosphorylation of Vps27 regulates ESCRT-I recruitment to endosomes, Mol. Biol. Cells 23 (20) (2012) 4054–4064.

[2] R. Kalluri, V.S. LeBleu, The biology, function, and biomedical applications of exosomes, Science 367 (6478) (2020) eaau6977.

[3] P.A. Gonzales, T. Pisitkun, J.D. Hoffert, D. Tchapyjnikov, R.A. Star, R. Kleta, N. S. Wang, M.A. Knepper, Large-scale proteomics and phosphoproteomics of urinary exosomes, J. Am. Soc. Nephrol. 20 (2) (2009) 363–379.

[4] C. Lässer, V.S. Alikhani, K. Ekström, M. Eldh, P.T. Paredes, A. Bossios, M. Sjöstrand, S. Gabrielsson, J. Lötvall, H. Valadi, Human saliva, plasma and breast milk exosomes contain RNA: uptake by macrophages, J. Transl. Med. 9 (1) (2011) 9.

[5] A. Poliakov, M. Spilman, T. Dokland, C.L. Amling, J.A. Mobley, Structural heterogeneity and protein composition of exosome-like vesicles (prostasomes) in human semen, Prostate 69 (2) (2009) 159–167.

[6] D.M. Goss, S.A. Vasilescu, G. Sacks, D.K. Gardner, M.E. Warkiani, Microfluidics facilitating the use of small extracellular vesicles in innovative approaches to male infertility, Nat. Rev. Urol. (2022).

[7] S. Zhand, K. Xiao, S. Razavi Bazaz, Y. Zhu, P. Bordhan, D. Jin, M.E. Warkiani, Improving capture efficiency of human cancer cell derived exosomes with nanostructured metal organic framework functionalized beads, Appl. Mater. Today 23 (2021), 100994.

[8] B. Hirshman, R. Kras, J. Akers, B. Carter, C.C. Chen, Extracellular vesicles in molecular diagnostics: an overview with a focus on CNS diseases, Adv. Clin. Chem. 76 (2016) 37–53.

[9] H. Valadi, K. Ekström, A. Bossios, M. Sjöstrand, J.J. Lee, J.O. Lötvall, Exosome-mediated transfer of mRNAs and microRNAs is a novel mechanism of genetic exchange between cells, Nat. Cell Biol. 9 (6) (2007) 654–659.

[10] M.P. Zaborowski, L. Balaj, X.O. Breakefield, C.P. Lai, Extracellular vesicles: composition, biological relevance, and methods of study, Bioscience 65 (8) (2015) 783–797.

[11] S. Zhand, A. Razmjou, S. Azadi, S.R. Bazaz, J. Shrestha, M.A.F. Jahromi, M. E. Warkiani, Metal–organic framework-enhanced ELISA platform for ultrasensitive detection of PD-L1, ACS Appl. Bio Mater. 3 (7) (2020) 4148–4158.

[12] J. De Toro, L. Herschlik, C. Waldner, C. Mongini, Emerging roles of exosomes in normal and pathological conditions: new insights for diagnosis and therapeutic applications, Front. Immunol. 6 (2015) 203.

[13] A. Möller, R.J. Lobb, The evolving translational potential of small extracellular vesicles in cancer, Nat. Rev. Cancer 20 (12) (2020) 697–709.

[14] J.S. Schorey, Y. Cheng, P.P. Singh, V.L. Smith, Exosomes and other extracellular vesicles in host–pathogen interactions, EMBO Rep. 16 (1) (2015) 24–43.

[15] K.M. Koo, P.N. Mainwaring, S.A. Tomlins, M. Trau, Merging new-age biomarkers and nanodiagnostics for precision prostate cancer management, Nat. Rev. Urol. 16 (5) (2019) 302–317.

[16] Z. Li, H. Cai, Z. Li, L. Ren, X. Ma, H. Zhu, Q. Gong, H. Zhang, Z. Gu, K. Luo, A tumor cell membrane-coated self-amplified nanosystem as a nanovaccine to boost the therapeutic effect of anti-PD-L1 antibody, Bioact. Mater. 21 (2023) 299–312.

[17] C. Théry, K.W. Witwer, E. Aikawa, M.J. Alcaraz, J.D. Anderson, R. Andriantsitohaina, A. Antoniou, T. Arab, F. Archer, G.K. Atkin-Smith, Minimal information for studies of extracellular vesicles 2018 (MISEV2018): a position statement of the International Society for Extracellular Vesicles and update of the MISEV2014 guidelines, J. Extracell. Vesicles 7 (1) (2018), 1535750.

[18] T. Shtam, R. Samsonov, R. Kamyshinsky, R. Pantina, N. Verlov, A. Vasiliev, A. Konevega, A. Malek, Exosomes: some approaches to cancer diagnosis and therapy, in: Proceedings of the AIP Conference, AIP Publishing LLC, 2017.

[19] Z. Li, X. Lai, S. Fu, L. Ren, H. Cai, H. Zhang, Z. Gu, X. Ma, K. Luo, Immunogenic cell death activates the tumor immune microenvironment to boost the immunotherapy efficiency, Adv. Sci. 9 (22) (2022), 2201734.

[20] A. Cimino-Mathews, E. Thompson, J.M. Taube, X. Ye, Y. Lu, A. Meeker, H. Xu, R. Sharma, K. Lecksell, T.C. Cornish, PD-L1 (B7-H1) expression and the immune tumor microenvironment in primary and metastatic breast carcinomas, Hum. Pathol. 47 (1) (2016) 52–63.

[21] M.N. Theodoraki, S.S. Yerneni, T.K. Hoffmann, W.E. Gooding, T.L. Whiteside, Clinical significance of PD-L1+ exosomes in plasma of head and neck cancer patients PD-L1+ exosomes in plasma of HNC patients, Clin. Cancer Res. 24 (4) (2018) 896–905.

[22] D.D. Taylor, C. Gercel-Taylor, MicroRNA signatures of tumor-derived exosomes as diagnostic biomarkers of ovarian cancer, Gynecol. Oncol. 110 (1) (2008) 13–21.

[23] A. Psyrri, T.Y. Seiwert, A. Jimeno, Molecular pathways in head and neck cancer: EGFR, PI3K, and more, Am. Soc. Clin. Oncol. Educ. Book 33 (1) (2013) 246–255.

[24] M. Tkach, J. Kowal, C. Théry, Why the need and how to approach the functional diversity of extracellular vesicles, Philos. Trans. R. Soc. Lond. B Biol. Sci. 373 (1737) (2018), 20160479.

[25] T.A. Hartjes, S. Mytnyk, G.W. Jenster, V. van Steijn, M.E. van Royen, Extracellular vesicle quantification and characterization: common methods and emerging approaches, Bioengineering 6 (1) (2019) 7.

[26] Y. Jia, Z. Ni, H. Sun, C. Wang, Microfluidic approaches toward the isolation and detection of exosome nanovesicles, IEEE Access 7 (2019) 45080–45098.

[27] M. He, J. Crow, M. Roth, Y. Zeng, A.K. Godwin, Integrated immunoisolation and protein analysis of circulating exosomes using microfluidic technology, Lab Chip 14 (19) (2014) 3773–3780.

[28] H. Zhang, D. Freitas, H.S. Kim, K. Fabijanic, Z. Li, H. Chen, M.T. Mark, H. Molina, A.B. Martin, L. Bojmar, Identification of distinct nanoparticles and subsets of extracellular vesicles by asymmetric flow field-flow fractionation, Nat. Cell Biol. 20 (3) (2018) 332–343.

[29] Y. Zhou, Z. Ma, M. Tayebi, Y. Ai, Submicron particle focusing and exosome sorting by wavy microchannel structures within viscoelastic fluids, Anal. Chem. 91 (7) (2019) 4577–4584.

[30] D. Yuan, Q. Zhao, S. Yan, S.Y. Tang, G. Alici, J. Zhang, W. Li, Recent progress of particle migration in viscoelastic fluids, Lab Chip 18 (4) (2018) 551–567.

[31] J.C. Contreras-Naranjo, H.J. Wu, V.M. Ugaz, Microfluidics for exosome isolation and analysis: enabling liquid biopsy for personalized medicine, Lab Chip, 17 (21) (2017) 3558–3577.

[32] F. Mirakhorli, S.S. Mohseni, S.R. Bazaz, A.A. Mehrizi, P.J. Ralph, M.E. Warkiani, Microfluidic platforms for cell sorting, in: G. Szekely, D. Zhao (Eds.), ‚Sustainable Separation Engineering, Wiley, , 2022, pp. 653–695.

[33] C. Chen, J. Skog, C.H. Hsu, R.T. Lessard, L. Balaj, T. Wurdinger, B.S. Carter, X. O. Breakefield, M. Toner, D. Irimia, Microfluidic isolation and transcriptome analysis of serum microvesicles, Lab Chip 10 (4) (2010) 505–511.

[34] S. Razavi Bazaz, A. Mashhadian, A. Ehsani, S.C. Saha, T. Krüger, M. Ebrahimi Warkiani, Computational inertial microfluidics: a review, Lab Chip, 20 (6) (2020) 1023–1048.

[35] C.L. Hisey, K.D.P. Dorayappan, D.E. Cohn, K. Selvendiran, D.J. Hansford, Microfluidic affinity separation chip for selective capture and release of label-free ovarian cancer exosomes, Lab Chip 18 (20) (2018) 3144–3153.

[36] S. Razavi Bazaz, O. Rouhi, M.A. Raoufi, F. Ejeian, M. Asadnia, D. Jin, M. Ebrahimi Warkiani, 3D printing of inertial microfluidic devices, Sci. Rep. 10 (1) (2020) 5929.

[37] S. Razavi Bazaz, N. Kashaninejad, S. Azadi, K. Patel, M. Asadnia, D. Jin, M. Ebrahimi Warkiani, Rapid softlithography using 3D-printed molds, Adv. Mater. Technol. 4 (10) (2019), 1900425.

[38] D. Di Carlo, Inertial microfluidics, Lab Chip, 9 (21) (2009) 3038–3046.

[39] S. Shin, D. Han, M.C. Park, J.Y. Mun, J. Choi, H. Chun, S. Kim, J.W. Hong, Separation of extracellular nanovesicles and apoptotic bodies from cancer cell culture broth using tunable microfluidic systems, Sci. Rep. 7 (1) (2017) 1–8.

[40] M.M. Bradberry, S. Mishra, Z. Zhang, L. Wu, J.M. McKetney, M.M. Vestling, J. J. Coon, E.R. Chapman, Rapid and gentle immunopurification of brain synaptic vesicles, J. Neurosci. 42 (17) (2022) 3512–3522.

[41] A. Säll, D. Corbee, S. Vikström, F. Ottosson, H. Persson, S. Waldemarson, Advancing the immunoaffinity platform AFFIRM to targeted measurements of proteins in serum in the pg/ml range, PLoS ONE 13 (2) (2018), e0189116.

[42] D. Lagundžin, K.L. Krieger, H.C.-H. Law, N.T. Woods, An optimized co-immunoprecipitation protocol for the analysis of endogenous protein-protein interactions in cell lines using mass spectrometry, STAR Protoc. 3 (1) (2022), 101234.

[43] S. Razavi Bazaz, A. Mihandust, R. Salomon, H.A.N. Joushani, W. Li, H.A. Amiri, F. Mirakhorli, S. Zhand, J. Shrestha, M. Miansari, B. Thierry, D. Jin, M. Ebrahimi Warkiani, Zigzag microchannel for rigid inertial separation and enrichment (Z-RISE) of cells and particles, Lab Chip 22 (21) (2022) 4093–4109.

[44] Y.T. Kang, T. Hadlock, S. Jolly, S. Nagrath, Extracellular vesicles on demand (EVOD) chip for screening and quantification of cancer-associated extracellular vesicles, Biosens. Bioelectron. 168 (2020), 112535.

[45] S.S. Kanwar, C.J. Dunlay, D.M. Simeone, S. Nagrath, Microfluidic device (ExoChip) for on-chip isolation, quantification and characterization of circulating exosomes, Lab Chip 14 (11) (2014) 1891–1900.

[46] F. Liu, O. Vermesh, V. Mani, T.J. Ge, S.J. Madsen, A. Sabour, E.-.C. Hsu, G. Gowrishankar, M. Kanada, J.V. Jokerst, The exosome total isolation chip, ACS Nano 11 (11) (2017) 10712–10723.

[47] Z. Zhao, Y. Yang, Y. Zeng, M. He, A microfluidic ExoSearch chip for multiplexed exosome detection towards blood-based ovarian cancer diagnosis, Lab Chip 16 (3) (2016) 489–496.

[48] B.H. Wunsch, J.T. Smith, S.M. Gifford, C. Wang, M. Brink, R.L. Bruce, R.H. Austin, G. Stolovitzky, Y. Astier, Nanoscale lateral displacement arrays for the separation of exosomes and colloids down to 20 nm, Nat. Nanotechnol. 11 (11) (2016) 936–940.

[49] Y.T. Kang, Y.J. Kim, J. Bu, Y.H. Cho, S.W. Han, B.I. Moon, High-purity capture and release of circulating exosomes using an exosome-specific dual-patterned immunofiltration (ExoDIF) device, Nanoscale 9 (36) (2017) 13495–13505.

[50] Y. Chen, Q. Zhu, L. Cheng, Y. Wang, M. Li, Q. Yang, L. Hu, D. Lou, J. Li, X. Dong, Exosome detection via the ultrafast-isolation system: EXODUS, Nat. Methods 18 (2) (2021) 212–218.

[51] J. Lim, M. Choi, H. Lee, J.Y. Han, Y. Cho, A novel multifunctional nanowire platform for highly efficient isolation and analysis of circulating tumor-specific markers, Front. Chem. 6 (2019) 664.